Journal of Computational Physics **150,** 468–481 (1999)
Article ID jcph.1999.6188, available online at http://www.idealibrary.com on IDEAL®

An Efficient Finite Element Method for Computing Spectra of Photonic and Acoustic Band-Gap Materials

I. Scalar Case

Waldemar Axmann[1] and Peter Kuchment[1]

Mathematics and Statistics Department, Wichita State University, Wichita, Kansas 67260-0033
E-mail: kuchment@twsuvm.uc.twsu.edu and wjaxmann@twsuvm.uc.twsu.edu

The paper describes an efficient finite element method for computing spectra of photonic and acoustic band-gap materials. In the photonic case only the scalar models are treated. The full vector model will be considered in the next publication.

Key Words: photonic crystals; finite element method.

1. INTRODUCTION

It was suggested in [29, 17] that complete band gaps could be created in the frequency spectrum of classical waves propagating in periodic composite materials by making appropriate choice of geometric and physical parameters. This means that waves of some frequencies cannot propagate in such a medium. These "band-gap materials" (also called "band-gap structures" or "photonic crystals") are optical or acoustic analogs of semiconductors, the major property of the latter being existence of band gaps in the energy spectrum of electrons. Band-gap media have attracted considerable attention recently due to a rich variety of important expected applications to high efficiency lasers, antennas, and other fields. Detailed information about theoretical and experimental study of such materials and their projected applications can be found in books and survey articles such as [3, 13, 16, 27, 28]. An extensive database of publications related to photonic crystals is maintained by Jon P. Dowling and Henry O. Everitt (http: //hwilwww.rdec.redstone.army.mil/MICOM/wsd/ST/RES/PBG/pbgbib.html).

[1] The work of both authors was partially supported by the the NSF under Grant DMS 9610444 and by a DEPSCoR grant.

0021-9991/99 $30.00

The band-gap structure of photonic crystals has been studied experimentally, numerically, and analytically. All of these studies confirmed the possibility of creating a complete band gap in the frequency spectrum. Probably the first analytic approach to high-contrast photonic crystals was developed in [7–9]. For the simplest geometries it led to asymptotic representations of spectra of photonic crystals in the high-contrast limit, which in turn led to the proof of existence of gaps in such spectra. These results and their further extension in [10, 11, 20] were also used in combination with methods of Rayleigh–Ritz type for numerical calculations (see examples of such applications in [6, 23, 24]). The main numerical methods used for computing spectra of infinite pure photonic crystals employ plane wave expansions. Consideration of truncated crystals or crystals with impurities usually requires additional tools. In spite of many successful computations, Fourier-type methods have several drawbacks, such as slow convergence of Fourier series and high demands for computer memory and speed. This makes development of alternative methods of computation desirable.

The purpose of this paper is to report an efficient finite element method for computing frequency spectra of classical waves in such periodic structures. We consider here only the scalar models of wave propagation, which describe electromagnetic waves in 2D photonic crystals and acoustic waves in 2D and 3D periodic media. The consideration of the full vector 3D model is planned for a subsequent publication. The paper is structured as follows. Section 2 contains a brief description of the mathematical model and some preliminary discussion of numerical methods. The algorithm is described in Section 3 and its performance is discussed in Section 4. The last section contains acknowledgments and a disclaimer.

After this work was done, the authors learned that D. Dobson at Texas A & M was simultaneously developing a similar (albeit not identical) algorithm [4].

2. THE MATHEMATICAL MODEL AND PRELIMINARY DISCUSSION

The mathematical model for spectral analysis of monochromatic electromagnetic waves in a periodic lossless non-magnetic dielectric material can be extracted from the standard macroscopic Maxwell equations [14], which can be written as

$$\begin{cases} \nabla \times \frac{1}{\varepsilon} \nabla \times \mathbf{H} = \lambda \mathbf{H} \\ \nabla \cdot \mathbf{H} = 0. \end{cases} \tag{2.1}$$

Here ε is the electric permittivity function, which describes the properties of the material. This function is assumed to be periodic with respect to a lattice in $\mathbb{R}^3$. The spectral parameter λ is

$$\lambda = \left(\frac{\omega}{c}\right)^2,$$

where ω is the frequency of the wave, and c is the speed of light.

When ε is periodic with respect to two variables and constant with respect to the third variable and when waves propagating only along the plane of periodicity are considered, the problem (2.1) splits into the direct sum of the following two scalar spectral problems in 2D (see, for instance, [16]):

$$-\nabla \cdot \frac{1}{\varepsilon} \nabla \psi = \lambda \psi \tag{2.2}$$

(so-called TE-polarization, or H-field) and

$$-\frac{1}{\varepsilon}\Delta\psi = \lambda\psi \tag{2.3}$$

(TM-polarization, or E-field). The same scalar spectral problems arise in 2D and 3D in studying the frequency spectra of acoustic waves in periodic media. In this paper we present an efficient method of computing spectra of periodic problems (2.2) and (2.3). A numerical treatment of the full vector spectral problem (2.1) is to be presented in the next paper.

There have been many successful computations of spectra of photonic band-gap structures (see, for instance, [3, 13, 16, 21, 27, 28], and references therein). Why then does one need another method? Most existing methods for infinite purely periodic crystals employ different versions of a plane wave expansion technique. In spite of successful computations, there are several problems with this approach.

First of all, the dielectric function ε is discontinuous, so Fourier-type expansions converge slowly. Many precautions must be taken in order to ensure that the calculated spectra are correct. For instance, a straightforward realization of plane wave expansion methods can lead to different numerical spectra for unitarily equivalent models (see [28]).

Another problem arises in trying to use thin dielectric structures of high refractivity index (which favors opening band gaps). It was shown in [7–9] that in this case, due to the effect of total internal reflection, many low frequency modes arise that are almost entirely localized in the dielectric region. Such modes are very hard to catch using the plane wave method, since important information about them will be hidden deep in the tails of Fourier expansions. This problem has not attracted much attention from researchers yet, since such high contrast "thin wall" materials probably are not currently technologically feasible. However, with advances in technology the manufacturing of such materials could become possible, posing a problem for Fourier-based methods.

Another difficulty with plane wave expansions is that the matrices arising in such methods are usually full. This makes the algorithms computationally expensive and significantly limits the number of modes that can be taken into account. For instance, as reported by the authors of the survey [28], with 100Mb memory only 41 expansion terms could be used per dimension in the 2D case and 11 terms per dimension in the 3D case.

The method described below has many advantages. It easily takes into account discontinuities in the dielectric function. The size of the mesh can be adjusted near expected singularities of solutions. The resulting matrices are very sparse, making memory limitations almost non-existent. The algorithm can be arranged in such a way that many computationally expensive steps like multiplication of large matrices, Cholesky decompositions, etc., are eliminated. Comparison of explicitly solvable cases and cases where the spectra have been previously computed by Fourier-type methods shows excellent agreement. There are additional possibilities of increasing the speed of this already fast algorithm even further. Finally, as we have already mentioned, the algorithm can be adjusted to work for the full 3D vector case, although it requires a different type of finite element method.

3. DESCRIPTION OF THE ALGORITHM

The algorithm utilizes a version of the finite element method. The theory (in particular, convergence) and practice of such methods for elliptic problems are rather well understood;

we refer the reader to the corresponding literature (see, for instance, [2, 15, 30]). We will describe here only the 2D case, since the scalar 3D case is handled similarly.

Consider first the divergent-type problem (2.2), which corresponds to the TE-polarization in the electromagnetic case:

$$-\nabla \cdot \frac{1}{\varepsilon(x)} \nabla \psi = \lambda \psi.$$

Here $\varepsilon(x) \geq 1$ is a periodic function. The algorithm handles arbitrary lattices of periods, but for simplicity of presentation we describe it only for the simple square lattice. In other words, we assume that the structure is 1-periodic with respect to each variable. Treatment of periodic problems requires utilization of the so-called Floquet–Bloch theory (see, for instance, [5, 18, 19, 25] for its description in the case of partial differential equations and [1] for applications in solid state physics). This theory is based on an analog of the Fourier transform, the latter being suitable mostly for constant coefficient equations. The meaning of this transform is expansion into irreducible representations of the lattice of periods. Let us provide some details for the above equation. Introducing the so-called quasimomentum vector k, we consider this problem on Bloch functions

$$\psi = e^{ik \cdot x} u(x),$$

where $u(x)$ is 1-periodic. The problem reduces to

$$-(\nabla + ik) \cdot \frac{1}{\varepsilon(x)} (\nabla + ik) u = \lambda u \tag{3.1}$$

on periodic functions u. According to the Floquet–Bloch theory (see [1, 5, 19, 25]), the spectrum of the original problem (2.2) in $L_2(\mathbb{R}^2)$ coincides with the union over $k \in B$ of the spectra of problems (3.1), where

$$B = \left\{ k \in R^2 \mid -\pi \leq k_j \leq \pi,\ j = 1, 2 \right\}$$

is called the Brillouin zone. In the presence of additional symmetries, the Brillouin zone can sometimes be replaced by a smaller, so-called reduced zone. One can rewrite (3.1) as

$$\int_{\mathbb{T}} \frac{1}{\varepsilon(x)} (\nabla + ik) u \cdot \overline{(\nabla + ik) v}\, dx = \lambda \int_T u \bar{v}\, dx.$$

Here $\mathbb{T}$ is the two-dimensional torus $\mathbb{T} = \mathbb{R}^2/\mathbb{Z}^2$, $\mathbb{Z}^2$ is the 2D integer lattice, u is the eigenmode, and v is an arbitrary periodic function from $H^1(\mathbb{T})$.

A mesh of triangular elements is then constructed on the torus $\mathbb{T}$. Basis functions, $\phi_j(x)$, are chosen to be linear on each element. Representing $u = \sum \xi_j \phi_j$ and then choosing $v = \phi_l$, we get a generalized eigenvalue problem

$$A(k)\xi = \lambda B \xi \tag{3.2}$$

on the corresponding subspace of piecewise linear functions in $L_2(\mathbb{T})$. Here

$$A_{jl} = \int_T \frac{1}{\varepsilon(x)} (\nabla + ik)\phi_j \cdot \overline{(\nabla + ik)\phi_l}\, dx$$

and

$$B_{jl} = \int_T \phi_j \bar{\phi}_l\, dx.$$

For the second scalar problem (TM-polarization),

$$-\nabla^2\psi = \lambda\varepsilon(x)\psi,$$

one similarly gets an analogous generalized eigenvalue problem with matrices A and B defined as

$$A_{jl} = \int_T (\nabla + ik)\phi_j \cdot \overline{(\nabla + ik)\phi_l}\, dx$$

and

$$B_{jl} = \int_T \varepsilon(x)\phi_j \bar{\phi}_l\, dx.$$

The matrix $A(k)$ is Hermitian and the matrix B is positive definite.

So, now the task is to solve numerically the generalized eigenvalue problem (3.2). Let $\lambda_j(k)$ be the jth eigenvalue of (3.2) considered as a function of k. It is called a band function or dispersion relation. The union of ranges of all band functions forms the spectrum of the original problem. In actual calculations one takes this union over a selected grid of points k in the Brillouin zone. This is exactly what our algorithm does.

3.1. *Mesh*

We used the mesh generator Easymesh 1.4 created by Bojan Niceno, University of Trieste, which produces high quality triangular 2D meshes in general domains. Easymesh also allows the introduction of different values of the dielectric constant in each element. In order to perform the computation needed for the photonic crystal spectra, the mesh must be periodic (i.e., it should be a mesh on the torus $\mathbb{T}$). An appropriate choice of input data ensures that the meshes produced by the Easymesh are periodic. Since each node in the meshes created by the generator has only about five to seven neighboring nodes, the resulting matrices are extremely sparse—only six to eight entries per row. Sparseness is very important for creating an efficient algorithm.

3.2. *Assembling and Storing the Matrices*

Computation of matrices A and B (which is called assembling in finite element methods) is straightforward according to the formulas introduced above. The matrix $A(k)$ is a quadratic function of the quasimomentum

$$A(k) = A_0 + \sum A_{1,j}k_j + A_2k^2.$$

We compute the constant matrices A_0, $A_{1,j}$, and A_2, and then for any given k assemble the matrix $A(k)$ according to this formula.

One of the major problems in computations of spectra of band-gap materials is the storage. In the finite element algorithm this problem is significantly reduced due to sparseness and becomes practically non-existent. Indeed, the rows and columns of matrices A and B have very few non-zero entries, whose locations are easy to determine. This means that if only non-zero elements of matrices are stored with corresponding pointers, then the storage

required for the matrices grows as $O(N)$ instead of $O(N^2)$, where N is the size of the mesh. Furthermore, computations with these matrices can be performed with many fewer operations than computations with the full matrices of the same size. This allows the use of much finer meshes and efficient computations for the 3D problem.

3.3. *Solving the Generalized Eigenvalue Problem*

The choice of a method for solving the generalized eigenvalue problem (3.2) is also very significant. Experimentation shows that standard eigenvalue codes are not efficient for matrices of the size we use. For instance, one of the standard approaches is to use the Cholesky decomposition of B,

$$B = GG^*,$$

where G is a lower triangular matrix with positive diagonal elements. Then the generalized spectral problem reduces to a standard one,

$$(G^{-1}AG^{*^{-1}})v = \lambda v.$$

However, the decomposition and multiplication destroy the sparseness of the matrices and thus the storage and speed advantages.

In computing spectra of photonic crystals, one is usually interested only in a small number (up to 10) of the lowest eigenvalues. The idea is to use a method that provides calculation of only such eigenvalues rather than attempting to compute all of them, and that efficiently utilizes sparseness of matrices involved. Subspace iteration methods are known to have these properties. We ended up using the simultaneous coordinate overrelaxation (SICOR) method (see [26] and references therein), which suits our purpose very well. This is a version of the subspace iteration method in which many computationally expensive steps can be avoided. We will now briefly describe the algorithm (the details and discussion can be found in [26]). Consider the generalized eigenvalue problem

$$A(k)\xi = \lambda B\xi.$$

Its smallest eigenvalue, λ_1, is equal to the minimum of the Rayleigh quotient

$$R(x) = \frac{(Ax, x)}{(Bx, x)}.$$

Furthermore, the vector which minimizes this value is a corresponding eigenvector. The coordinate relaxation (CR) method starts with some initial guess $x \neq 0$ and the minimum of the Rayleigh quotient is sought iteratively by changing x one component at a time. So in each cycle of iteration the n problems ($j = 1, \ldots, n$) of minimizing $R(x^c)$ over the set of vectors $x^c = \phi x + \psi e_j$ are solved. Here ϕ and ψ are complex scalars and e_j is the jth standard basis vector. Solving each of these minimization problems amounts to solving a two-dimensional generalized eigenvalue problem (see details in [26]). Completing this entire process once for each component of x constitutes a single iterative step of CR.

To improve the convergence rate of CR one turns to the coordinate overrelaxation (COR) method. COR does to CR what the more well known SOR (successive overrelaxation) does to SR (successive relaxation): it adds a relaxation parameter ω to the problem with the hope of speeding things up (see, for instance, [12, Sect. 10.1.4]). Instead of setting $x^c = \phi x + \psi e_j$, COR sets $x^c = \phi x + \omega\psi e_j$. We then adjust ω in order to obtain faster convergence.

SICOR (simultaneous coordinate overrelaxation) marries COR to a form of subspace iteration in order to simultaneously calculate p lowest eigenvalues. In SICOR one starts with p linearly independent initial vectors arranged in an $n \times p$ matrix $X = (x_1, \ldots, x_p)$. In each iteration one performs a COR step on each of these vectors to obtain a new set of vectors X^c and their Rayleigh quotients. In order to keep all p vectors from converging to the lowest eigenvector a Ritz step is inserted in each iteration. The Ritz step produces a p-dimensional subspace that is the best approximation to the p smallest eigenvectors. In this step a new set of linearly independent vectors X^r is formed by taking linear combinations of the vectors X^c produced by the COR step. The coefficients of this linear combination are chosen so that the Rayleigh quotients take on their p stationary values in increasing order. To achieve this goal, one must solve the $p \times p$ generalized eigenvalue problem

$$A_1 y = \Lambda B_1 y,$$

where $A_1 = X^{c^*} A X^c$ and $B_1 = X^{c^*} B X^c$. Since p is a small number (in our calculations we chose $p = 13$), this step is computationally inexpensive.

4. PERFORMANCE OF THE ALGORITHM

In order to check that the algorithm works correctly, we have tested it against several cases in which a few band functions were computed using different methods. The results show very good agreement. Discussed below are some of these comparisons.

Consider, for instance, the situation studied in [22]: dielectric rods of circular cross section and dielectric constant ε embedded into air (dielectric constant 1). The rods are placed in such a way that the rods' axes intersect the plane of periodicity at the points of a regular triangular lattice (see Fig. 1). The length of each side of the triangles is a. This

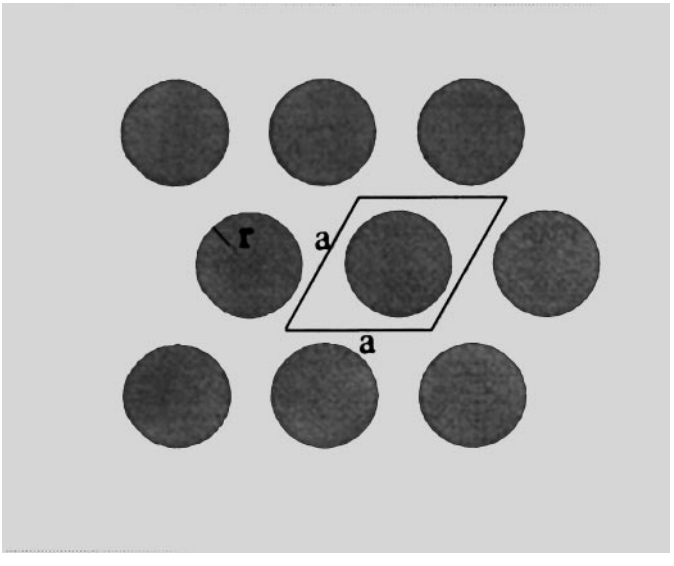

FIG. 1. The geometry of the material. The dark areas are filled with the dielectric.

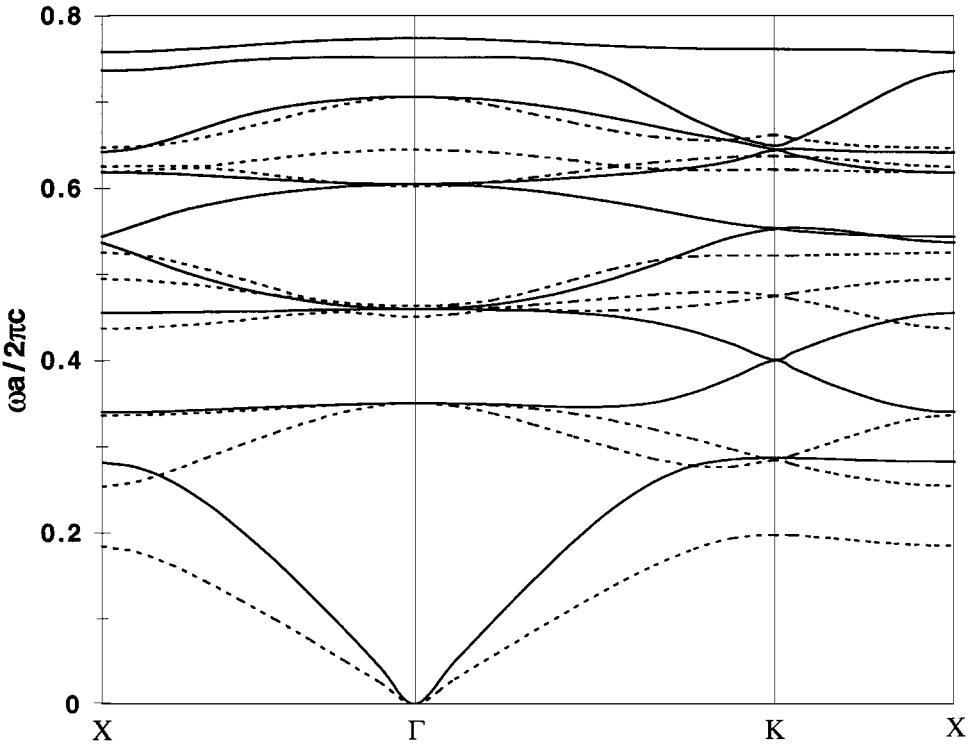

FIG. 2. Band functions for dielectric rods with $\varepsilon = 14$ and $f = 0.431$ embedded into air.

lattice consists of integer linear combinations of vectors $a(1, 0)$ and $a(0.5, 0.5\sqrt{3})$. We use the filling fraction f instead of the radius to characterize the size of the rods. The filling fraction represents the fraction of the volume occupied by the rods.

Figure 2 represents the graphs of the first nine band functions (dispersion relations) for both TM (dashed line) and TE (solid line) polarizations for the case $\varepsilon = 14$ and $f = 0.431$. These functions, as is customary in physics, are graphed over the sides of the triangle ΓKX in the quasimomentum space (see Fig. 3). The frequencies are measured in the dimensionless units $\omega a/2\pi c$. The solid lines correspond to the results presented in Fig. 1(a) of [22]. Comparing the figures, one can see that the results agree well. We also provide in Table I the list of several first bands of the spectrum for both polarizations.

The results presented in Fig. 4 correspond to $\varepsilon = 5$ and $f = 0.169$. The dashed lines compared with graphs in Fig. 1(b) of [22] also show very good agreement. Table II shows several spectral bands for this case.

Figure 5 presents the band structure for the case of air columns ($\varepsilon = 1$) embedded into the dielectric with $\varepsilon = 12.5$ and with the filling fraction $f = 0.6$. The solid lines compared with Fig. 2(a) in [22] also show good agreement. In Table III we present the first five spectral bands for this case.

Also, we have done calculations for the case of the square structure considered in [6, 23, 24]. This structure is shown in Fig. 6. The period is equal to 1; the thickness of the dark area is 0.1. The dark area is occupied by a dielectric with $\varepsilon = 20$, while the white area is filled with air. Table IV shows the results of computing several spectral bands for this case in comparison with computations in [6, 23, 24]. The second column shows the first three

TABLE I

	TM		TE	
Band No.	Beginning	End	Beginning	End
1	0	0.19673	0	0.286089
2	0.253637	0.350038	0.339239	0.39917
3	0.283547	0.350039	0.399618	0.459315
4	0.436544	0.47423	0.459318	0.552086
5	0.460511	0.494484	0.544018	0.604957

TABLE II

	TM		TE	
Band No.	Beginning	End	Beginning	End
1	0	0.391639	0	0.576372
2	0.518225	0.728482	0.535526	0.771784
3	0.591172	0.772109	0.591576	0.93831
4	0.772121	0.96335	0.855493	0.974257
5	0.943789	1.050677	1.018472	1.127292

TABLE III

	TM		TE	
Band No.	Beginning	End	Beginning	End
1	0	0.238094	0	0.246056
2	0.238375	0.356644	0.413545	0.498277
3	0.359904	0.406239	0.435281	0.58265
4	0.406246	0.500043	0.577062	0.631607
5	0.501225	0.570934	0.624439	0.660613

TABLE IV

Band No.	TE spectrum		
1	[0, 0.30697]	[0, 0.30738]	[0, 0.30792]
2	[0.46182, 0.58973]	[0.4621, 0.59038]	[0.46237, 0.58917]
3	[0.5281, 0.65176]	[0.52882, 0.65176]	[0.52851, 0.65205]
Band No.	TM spectrum		
1	[0, 0.2366]	[0, 0.24189]	[0, 0.24201]
2	[0.2586, 0.35907]	[0.2586, 0.35907]	[0.25907, 0.35939]
3	[0.29519, 0.37831]	[0.29476, 0.38691]	[0.29579, 0.38672]

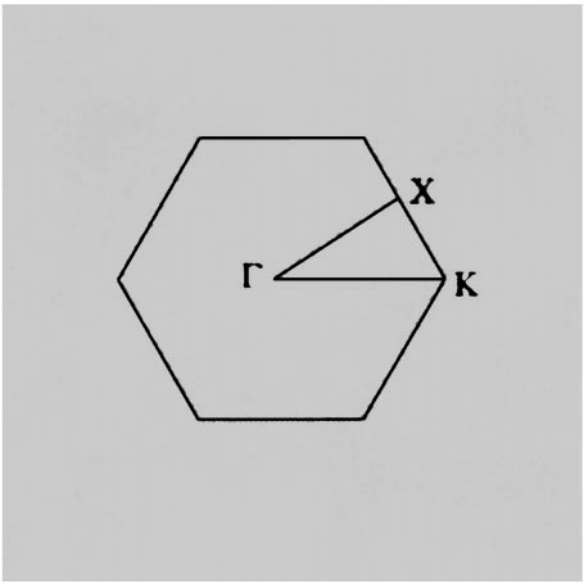

FIG. 3. The Brillouin zone with the $\Gamma K X$ triangle.

zones obtained in [6], and the third column those obtained in [23, 24]. The last column presents the results of our calculations.

One can see extremely good agreement of the results. We should mention that computations done in [6, 23, 24] were based on the square geometry only and used existence of an

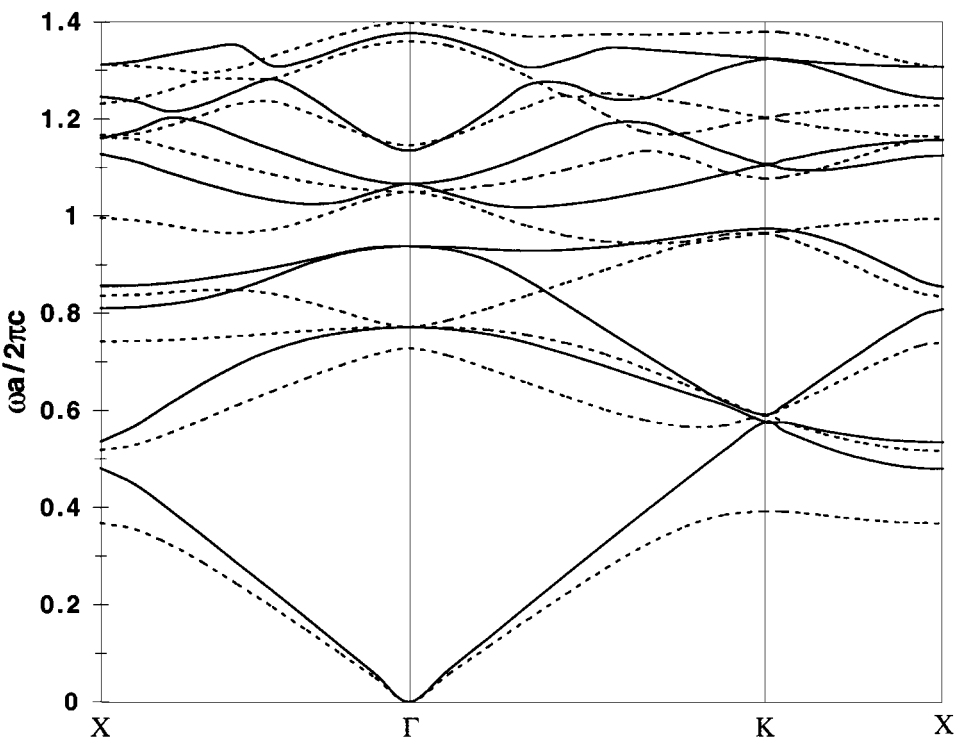

FIG. 4. Band functions for dielectric rods with $\varepsilon = 5$ and $f = 0.169$ embedded into air.

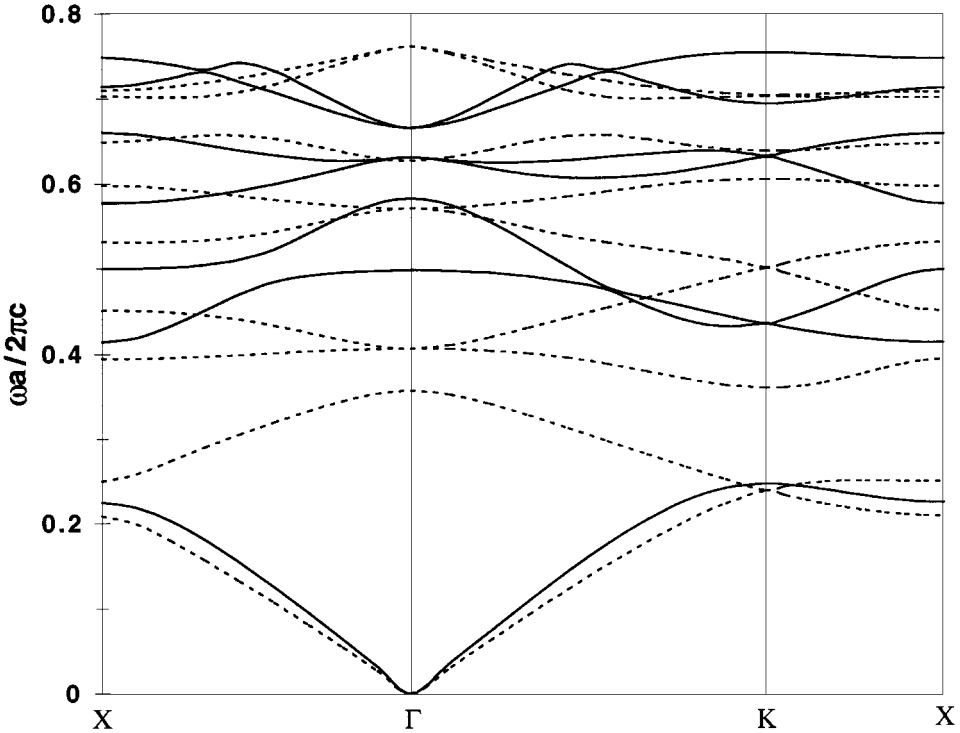

FIG. 5. Band functions for air columns embedded into the dielectric with $\varepsilon = 12.5$ and $f = 0.6$.

explicitly solvable problem in the vicinity of the spectral problem of interest. This approach does not work for general geometries.

Another comparison was done with some of the computations for 2D structures presented in the survey [28]. The results obtained by our method agree well with those described in [28].

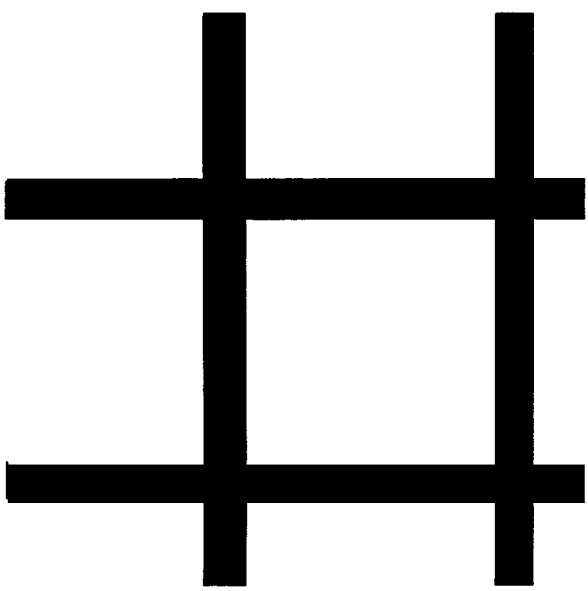

FIG. 6. The square structure. Dark areas are filled with the dielectric.

TABLE V
Algorithm's Performance Data

Mesh size	Memory used (Kb)	Running time (min)	No. of iterations
207	1,208	1.25	24
773	1,768	5.7	28
2,987	3,468	27	35
11,719	12,600	207	68

In order to test the performance of the algorithm in 3D, we applied it to the explicitly solvable case of a homogeneous medium in 3D. This problem is much more demanding in terms of memory and speed of computations, due to three dimensionality. Comparison of numerical and analytic results revealed the average relative error of 1.1% and the maximum relative error of 3% for a rather small mesh size of 20^3 nodes.

The code was written in Objective C and the calculations were performed on a DEC Alpha 533 workstation running LINUX. Table V contains data about the performance of the algorithm during the calculation of 13 band functions (only 9 of which are used) for a single polarization, with different mesh sizes, on a 9×9 grid in the Brillouin zone.

Preconditioners analogous to those used in [4] would probably lead to additional reduction of the running time. Note that the memory used increases only as $O(N)$ and is nowhere near the 128M of memory available on this computer. The running time seems to increase as $O(N \ln N)$, although additional data for larger meshes would be needed to confirm this.

The algorithm was run until the absolute change in the eigenvalues became less than 10^{-5} (we remind the reader that dimensionless units were used for the spectrum).

It is also interesting to observe how the results change with the size of the mesh. Table VI shows the percentage change between the eigenvalues obtained using different mesh sizes. This table shows that for the type of computations performed a mesh of size 3006 is quite sufficient. In fact, even the coarse mesh of size 227 (for which the running time is less than a minute) provides a general idea of the spectrum.

The role of the relaxation parameter w is very significant for convergence (see the corresponding discussion in the Section 5.4 of [26] and in [12, Sect. 10.1.4]), and some experimentation is needed in order to choose its value. We found the following best choices of w depending on the mesh size: $w = 1.58$, 1.64, 1.86, and 1.90 for the meshes of sizes 227, 796, 3006, and 11,817 correspondingly.

TABLE VI
Algorithm's Convergence Data

Mesh sizes	Maximum % change TM	Average % change TM	Maximum % change TE	Average % change TE
227 and 796	10.9	4.2	11.6	6.36
796 and 3006	2.4	1.0	2.9	1.6
3006 and 11,817	0.7	0.3	1.3	0.57

ACKNOWLEDGMENTS AND DISCLAIMER

The authors express their gratitude to Professor. D. Dobson for information about his work, Dr. L. Kunyansky for useful discussions, and the reviewers for important comments. This research was partly sponsored by the NSF through Grant DMS 9610444 and by the Department of Army, Army Research Office, through a DEPSCoR grant. The authors thank the NSF and the ARO for this support. The content of this paper does not necessarily reflect the position or the policy of the federal government, and no official endorsement should be inferred.

REFERENCES

1. N. W. Ashcroft and N. D. Mermin, *Solid State Physics* (Holt, Rinehart & Winston, New York/London, 1976).
2. P. G. Ciarlet, *The Finite Element Method for Elliptic Problems* (Elsevier North-Holland, Amsterdam, 1978).
3. Development and applications of materials exhibiting photonic band gaps, *J. Opt. Soc. Am. B* **10**, 280 (1993).
4. D. Dobson, An efficient method for band structure calculations in 2D photonic crystals, *J. Comput. Phys.* **149**, 363 (1999).
5. M. S. P. Eastham, *The Spectral Theory of Periodic Differential Equations* (Scottish Acad. Press, Edinburgh/London, 1973).
6. A. Figotin and Yu. Godin, Computation of spectra of some 2D photonic crystals, *J. Comput. Phys.* **136**, 585 (1997).
7. A. Figotin and P. Kuchment, Band-gap structure of spectra of periodic and acoustic media. I. Scalar model, *SIAM J. Appl. Math.* **56**, 68 (1996).
8. A. Figotin and P. Kuchment, Band-gap structure of spectra of periodic and acoustic media. II. 2D photonic crystals, *SIAM J. Appl. Math.* **56**, 1561 (1996).
9. A. Figotin and P. Kuchment, 2D photonic crystals with cubic structure: Asymptotic analysis, in *Wave Propagation in Complex Media*, IMA Volumes in Math. and Appl., Vol. 96, edited by G. Papanicolaou (Springer-Verlag, New York, 1997), p. 23.
10. A. Figotin and P. Kuchment, Spectral properties of classical waves in high contrast periodic media, *SIAM J. Appl. Math.* **58**, 683 (1998).
11. A. Figotin and P. Kuchment, Asymptotic models of high contrast periodic photonic and acoustic media, in preparation.
12. G. H. Golub and C. F. Van Loan, *Matrix Computations*, 3rd ed. (Johns Hopkins Univ. Press, Baltimore/London, 1996).
13. P. M. Hui and N. F. Johnson, Photonic band-gap materials, in *Solid State Physics* (Academic Press, New York, 1995), Vol. 49, p. 151.
14. J. D. Jackson, *Classical Electrodynamics* (Wiley, New York, 1975).
15. J. Jin, *The Finite Element Method in Electromagnetics* (Wiley, New York, 1993).
16. J. D. Joannopoulos, R. D. Meade, and J. N. Winn, *Photonic Crystals. Molding the Flow of Light* (Princeton Univ. Press, Princeton, NJ, 1995).
17. S. John, Strong localization of photons in certain disordered dielectric superlattices, *Phys. Rev. Lett.* **58**, 2486 (1987).
18. P. Kuchment, Floquet theory for partial differential equations, *Russian Math. Surveys* **37**, No. 4, 1 (1982).
19. P. Kuchment, *Floquet Theory for Partial Differential Equations* (Birkhäuser Verlag, Basel, 1993).
20. P. Kuchment and L. Kunyansky, Spectral properties of high contrast band-gap materials and operators on graphs, *Experiment. Math.* **8**, in press (1999).
21. K. M. Leung and Y. F. Liu, Full vector wave calculation of photonic band structures in face-centered-cubic dielectric media, *Phys. Rev. Lett.* **65**, 2646 (1990).
22. M. Plihal and A. A. Maradudin, Photonic band structure of two-dimensional systems: The triangular lattice, *Phys. Rev. B* **44**, 8565 (1991).
23. I. Ponomarev, Separation of variables in the computation of spectra of 2D photonic crystals, *SIAM J. Appl. Math.*, to appear.

24. I. Ponomarev, *Numerical Analysis of Problems of Tomography, Radiation Treatment, and Photonic Crystals Theory*, Ph.D. thesis (Wichita State University, Wichita, KS, 1997).
25. M. Reed and B. Simon, *Methods of Modern Mathematical Physics*, Vol. IV, *Analysis of Operators* (Academic Press, New York, 1978).
26. H. R. Schwarz, *Finite Element Methods* (Academic Press, London, 1988).
27. C. M. Soukoulis (Ed.), *Photonic Bands and Localization* (Plenum, New York, 1993).
28. P. R. Villaneuve and M. Piché, Photonic band gaps in periodic dielectric structures, *Prog. Quant. Electr.* **18**, 153 (1994).
29. E. Yablonovitch, Inhibited spontaneous emission in solid-state physics and electronics, *Phys. Rev. Lett.* **58**, 2059 (1987).
30. O. C. Zienkiewicz and R. L. Taylor, *The Finite Element Method* (McGraw–Hill, New York, 1989).